Earth Science Research; Vol. 4, No. 1; 2015
ISSN 1927-0542 E-ISSN 1927-0550
Published by Canadian Center of Science and Education

Geochemical and Isotope Sr-Nd Character of Dschang Biotite Granite: Implications for the Pan-African Continental Crust Evolution in West-Cameroon (Central Africa)

Kwékam Maurice[1,2], Hartmann Gerald[2], Njanko Théophile[1,3], Tcheumenak Kouémo Jules[1], Fozing Eric Martial[1] & Njonfang Emmanuel[4]

[1] Laboratoire de Géologie de l´Environnement (LGE), Faculté des Sciences, Université de Dschang, B.P. 67 Dschang, Cameroun

[2] Geowissenschaftliches Zentrum Göttingen, Georg-August-Universität Göttingen, Goldschmidt-Straße 1, 37077 Göttingen, Deutschland

[3] Ministère de la Recherche Scientifique et de l'Innovation, DPSP/CCAR, B.P. 1457, Yaounde, Cameroon

[4] Laboratoire de Géologie, Ecole Normale Supérieure, Université de Yaoundé I, B.P. 47, Yaounde, Cameroon

Corresponding author: Kwékam Maurice, Département Sciences de la Terre, Université de Dschang, Cameroun. Tel: 237-677-516-684. E-mail: mkwekam@yahoo.fr

Received: November 11, 2014 Accepted: December 2, 2014 Online Published: January 25, 2015

doi:10.5539/esr.v4n1p88 URL: http://dx.doi.org/10.5539/esr.v4n1p88

Abstract

The biotite granite of Dschang composing of quartz, feldspar and biotite, is a haplogranite I-type calc-alkaline granitoid. It is weakly peraluminous with a ferroan affinity and exhibits fractionated feature. This granite was generated at the minimum temperature and pressure of crystallization of 650°C/4 Kb. Its emplacement is syn-central Cameroon shear zone like most of post-collisional granitoids of the Pan-African fold belt in central Africa, and it displays N-S to NNE-SSW magmatic foliation dipping 30° to 60° towards W or WNW. The evolution of the major elements shows a generalized decrease correlation trends look firstly like fractional crystallization. The depleted Sr content related to decreasing Al_2O_3 and CaO concentrations, indicate the role played by plagioclase during differentiation. The trace elements normalized to the primitive mantle, show negative anomalies out of Nb, Ta, Sr and Ti, and positive anomalies out of Ba, Rb, Th, comparable with those of the continental crust. The isotopic data Sr-Nd are rather homogeneous suggesting a single source for the biotite granite of Dschang. $\varepsilon_{Nd600Ma}$ (- 16 to -18) and T_{DM} (1.9 to 2.1 Ga) confirm the formation of the magma of the biotite granite of Dschang starting from an old Paleoproterozoic crust by partial melting around 600 Ma. This melting which seems to have spread in the area and at several levels of the continental lithosphere, hence magmas were mixing throughout their evolution, considering the diversity of the granites and their sources, is certainly caused by great movements along CCSZ, at the post-collisional period of Pan-African orogenesis in central Africa.

Keywords: biotite granite, ferro-potassic calc-alkaline, partial melting, Paleoproterozoic crust, syn-shear post-collisional, Pan-African

1. Introduction

The biotite granite of Dschang is part of numerous late Pan-African granitic plutons that occur to the centre domain (Fig. 1) of Central Pan-African fold belt (CPAFB) in Cameroon. These massifs outcrops generally along the central Cameroon shear zone (CCSZ, N70°, Fig. 1). The region of Dschang located on the SW extension of the Tcholliré Banyo shear zone (TBSZ, Fig. 1), is particular interest to share its position at the junction of E-W to ENE - WSW structures of the Central Pan-African fold belt and N-S structures of the Eastern Nigeria Trans-Saharan Pan-African fold belt. Despite the large number of granitic massive in the SW region of this belt (western Cameroon), very few have been studied in detail. Even though, study of leucogranites that outcrop along a shear zone can allow more information about evolution of the crust or magmas generation and process.

The biotite granite of Dschang seems to be resulted from the high-K calc-alkaline post-collisional magmatic activities along of CCSZ. This magmatism, dated at 630 – 540 Ma (Toteu et al., 2004, Kwékam et al., 2013) is a major feature of the central domain of the Pan-African fold belt in Cameroon. Key issues related to the amount of remobilised crust in the source of the magmas, the age diversity and also their actual location in the Central

African mobile belt (Fig. 1b). This belt is considered as resulting from the convergence of the Congo and West-African cratons with the Saharan metacraton during the amalgamation of the Gondwana supercontinent (Abdelsalam et al., 2002).

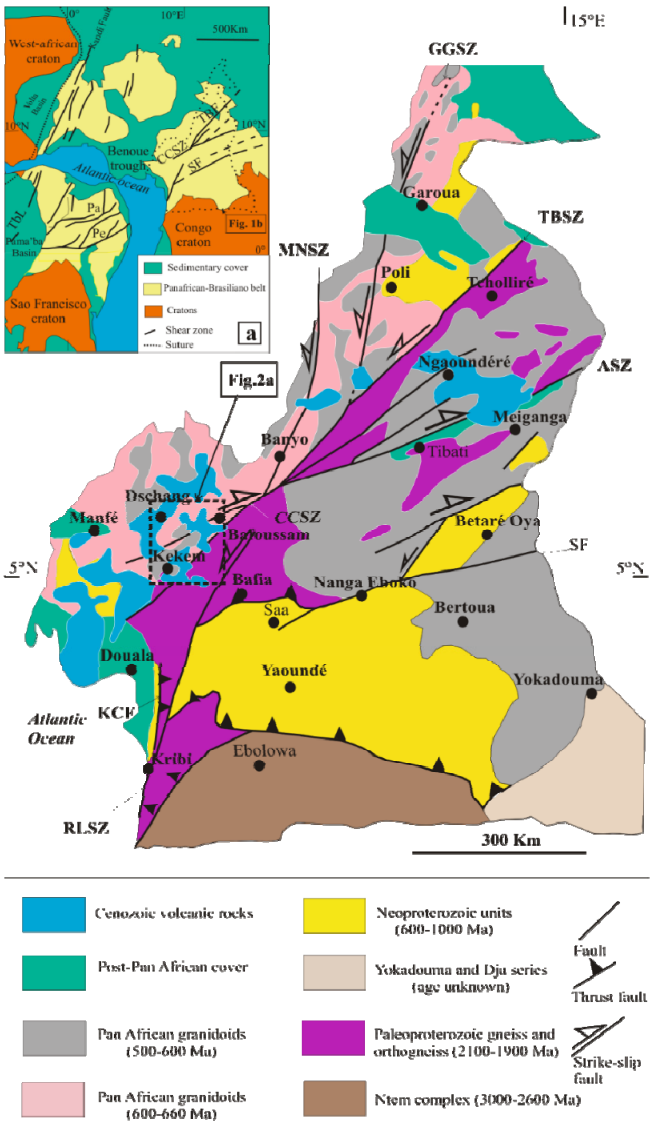

Figure 1.

(a) Geological sketch map of west-central Africa and northern Brazil with cratonic masses and the Pan-African-Brasiliano provinces of the Pan-gondwana belt in a Pangea reconstruction; modified from Castaing et al. (1994) and Abdelsalam et al. (2002). TBSZ: Tcholliré-Banyos hear zone, CCSZ: Central Cameroon shear zone, SF: Sanaga fault, ASZ: Adamaoua shear zone, Pa: Patos shear zone, Pe: Pernambuc shear zone, Tbl: Transbrasiliano lineament, Dashed outline roughly outline marks the political boundary of Cameroon, (b) geological sketch map of Cameroon showing from the major lithotectonic domains (After Toteu et al., 2001; Ngako et al., 2008). GGSZ: Godé-Gormaya shear zone, MNSZ: Mayo Nolti shear zone, RLSZ: Rocher de Loup shear zone, KCF: Kribi-Campo fault.

On the northern margin of the Congo craton in West Cameroon, the post-collisional Pan-African biotite granite of Dschang outcroups in migmatitic gneiss. This biotite granite has been previously interpreted as the product of crust recycled (Kwékam, 2005). However, proposed geodynamical models for most Cameroonian magmatic rocks point to a collisional setting within the former active margin (Ngako, 1999, Ngako et al., 2008; Toteu et al., 2004) or a post-collisional setting within the former passive margin (metacratonization of the northern boundary of the Congo craton; Kwékam et al., 2010). In this paper, field work, whole-rock major and trace elements geochemistry, and Rb-Sr and Sm-Nd isotopic data have been performed to determine more tightly the petrogenesis and geodynamical setting of this leucogranite. That´s the whole point of this study what the

discussion lead us to propose the place of bioitite granite of Dschang in the Pan-African continental crust evolution in West-Cameroon as well as in Central African fold belt.

2. Geological Setting

The Neoproterozoic Pan-African belt in West Cameroon comprises granito-gneissic units intruded by mafic to felsic plutons (including the biotite granite of Dschang) and overlain by Cenozoic to actual volcanic complexes (Fig.1b).

Four Pan-African regional tectonic phases have been recognized in Cameroon (Toteu et al., 2004). The D_1 would correspond to early Pan-African nape tectonics, verging east. The D_2 deformation is considered to be the result of an E-W regional shortening direction inducing a NE-SW transcurrent movement. Both D_1 and D_2 phases are associated with a N110-140°E stretching lineation. The D_3 phase is related to sinistral movements along the N-S to NE-SW shear zones. The final D_4 phase is characterized by N80-110°E dextral and N160-180°E sinistral shear zones. The D_1-D_2 phase are continued to the 635 – 615 Ma age range, the D_3 to the 600-580 age range and the D_4, poorly dated, is older than 545 Ma (Toteu et al., 2004 and references therein). These four phases, associated to collisional and post-collisional evolution in the Cameroon domain, have been more recently identified as corresponding to three successive tectonic events (Ngako et al., 2008): (1) crustal thickening (ca 630-620 Ma) including the thrusting (D_1) and shortening (D_2) of Toteu et al. (2004); (2) the left lateral wrench movements (613-585 Ma) among which the Sanaga shear zone, corresponding to D_3 of Toteu et al. (2004); (3) the right lateral wrench movements (ca 585-540 Ma) mainly marked by the CCSZ. The tectonic evolution of the Pan-African belt in central and southern Cameroon is characterized by transpression regime, because of coeval shear and thrust kinematic interactions. The resulting structures include the N70°E sinistral shear zones of central Cameroon (CCSZ and Sanaga fault) and the granulitic and migmatitic thrust sheets overriding the Congo craton (Ngako et al., 2008).

On a rheologic view, the PBCA in Cameroon is constituted of three units (Liégeois et al., 2013): (1) a cratonic unit in the south (part of the Congo craton); (2) a Pan-African metacratonic unit in the centre and (3) a Pan-African non metacratonic unit in the north. The Pan-African metacratonic and non metacratonic units are separated by the CCSZ that therefore constitute the transitional area between the two units. This view is locally documented by Tcheumenak Kouémo et al. (2014) for the Fodjomekwet-Fotouni shear zone that is a SW section of CCSZ. The PBCA is divided into three lithotectonic domains: a southern domain; a central domain and a northern domain (Penaye et al., 1993; Toteu et al., 2001).

The central domain is characterised by two major shear zones: the Sanaga Shear Zone (SSZ) and the Central Cameroon Shear Zone (CCSZ, Fig. 1b) and dominated by granitoid massifs. Detailed geological studies of some syntectonic Pan-African granitoids in the central domain of Cameroon (Kwékam et al., 2010; 2013; Nguiessi-Tchamkam et al., 1997; Tagne-Kamga et al., 1999; Tagne-Kamga, 2003; Njanko et al., 2006; Djouka-Fonkwé et al., 2008) show that they are essentially High-K calc-alkaline to shoshonitic and broadly elongated and aligned NE-SW, consistent with their successive emplacement coeval with oblique sinistral shear zones formed during an earlier deformation phase (Ngako, 1999; Tcheumenak Kouémo et al., 2014).

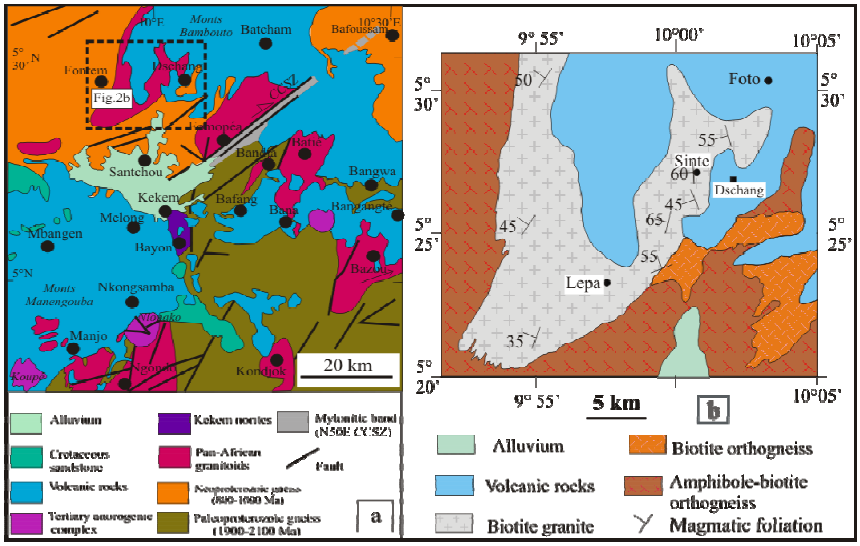

Figure 2.

(a) Extract of West-Cameroon geological map from Dumort (1968) modified from Kwékam et al. (2013), showing the locality of the Dschang granite and its neighbouring plutons and (b) Dschang granite geological map.

In the Dschang area, biotite and hornblende orthogneisses country rocks of biotite granite are affected by the shortening phase of crustal thickening. The foliation planes S1 are mainly oriented WNW-ESE (N110°E) and associated with P1 asymmetric folds (sinistral shear) and a stretching mineral lineation of the same orientation. They are often affected by P2 asymmetric folds associated with N70°E dextral shear and are cut by N70°E leucogranite dyke corresponding to the second tectonic event. The biotite granite develops a N-S magmatic foliation and is partly covered by volcanic rocks of Mount Bambouto (Fig. 2b). It is limited in places (borders south and southeast) by biotite orthogneisses characterized by large nodules of magnetite and a fine schistosity.

3. Structural

The magmatic fabrics in the biotite granite of Dschang are defined by platy megacrysts of alkali feldspar, schlieren of biotite and/or spindle-shaped enclaves. The main direction of the magmatic foliation is N-S to NNE-SSW with a dip of 30° to 60° towards W or WNW. This orientation is locally disrupted by xenoliths of gneissic rocks of various sizes or syn-magmatic shear that create nested flowage (imbricated structures, Fig. 3a). These structures of syn-magmatic shear in the same direction (roughly EW) are also observed in the Batié granite and the Fomopéa complex (Kwékam, 1993; Kwékam et al., 2010). Their orientation corresponds to that of the CCSZ described by Ngako et al. (2008).

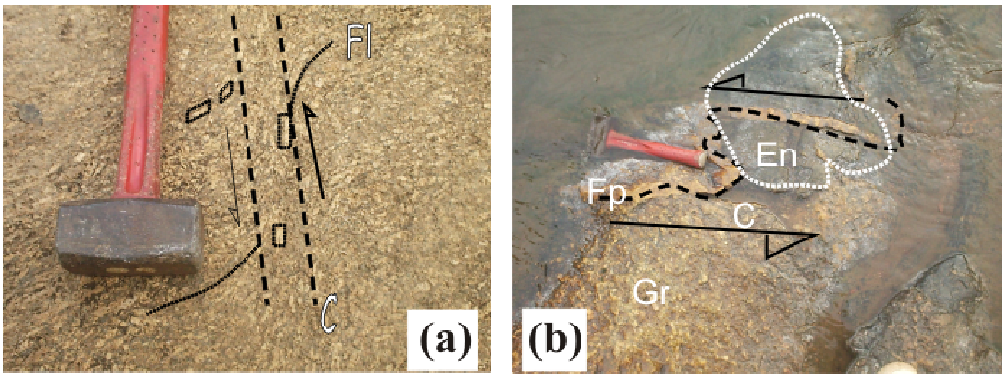

Figure 3. Field pictures of two outcrops

(a) syn-magmatic sinistral ductile shear fault “C” affecting the principal magmatic foliation “Fl”, some tabular feldspar crystals are marked to appreciate their orientation inside the protodike, (b) Dissymetrical folding of quartz vein “Fp” associated to sinistral N135E fault, “Gr” deformed granite, “En” micro-granitic enclave.

The post-magmatic deformation is marked by an extensive network of fractures; the most significant is defined by a band of N135°E sinistral deformation (Fig. 3b). The quartz vein pleated asymmetrically in the vicinity of this band (Fig. 3b), shows anticlockwise motion of shear. The biotite granite Dschang seems to undergo three phases of deformation. A first deformation (N-S to NNE-SSW) by flow in the viscous state related to its emplacement accompanied by a second still in the viscous state. This second strain secant to the first is an evidence of the existence a regional ENE-WSW shearing deformation during the emplacement of granite of Dschang, which correspond to CCSZ, (Fig. 1a) of Ngako et al. (2008). The third plastic to brittle deformation associated fault and fold, with dominated direction NW-SE is late-to post - magmatic.

All these structural elements give to the biotite granite of Dschang the syn-kinematic characteristic.

4. Petrography

The biotite granite of Dschang outcrops in metric balls and slabs or cutting veins in the orthogneisses and isolated sometimes the irregular and elongated or angular enclaves. The boundary between granite and orthogneisses is generally vague and often is characterized by migmatization structures. It is fairly homogeneous granite and contains dark fine-grained enclaves. These enclaves occur as centimetre to meter lens with the same mineralogical composition as granite host, they can be as streaks and clusters of biotite few centimetres long. In this work the biotite granite and fine-grained enclaves are studied.

The biotite granite of Dschang is a leucocratic fine-grained to coarse granite. Its mineralogical composition is fairly homogeneous, quartz (25 -30%), feldspar (24 to 27%), plagioclase (35 - 39%), biotite (8 to 12%) and accessory minerals (titanite, apatite, zircon, oxide iron, pyrite). Fine-grained enclaves are richer in biotite (12%) and plagioclase (39%) than in samples of feldspar megacrysts (8%) and (25%) respectively. Some tablets of alkali feldspars may reach 4 cm x 1.5 cm in size in the porphyritic type. These megacrysts of feldspar are often joined together by syneusis or twinning of the Carlsbad and contain macroscopic and microscopic inclusions of biotite and titanite. The alkali feldspar is orthoclase (Or_{92-95}), sub-euhedral to euhedral, twinned Carlsbad and albite or pericline, and sometimes all three at once. The plagioclase is oligoclase (An_{23-29}) in the enclaves and albite-oligoclase (an_{18-24}) in the granite. The crystals are subidiomorphic and display polysynthetic albite twins. Some plagioclase crystals show mechanical twins type albite. It is altered to epidote.

Biotite is greenish to light brown occur either as isolated crystals or in combination of two or three flakes which are generally oriented in the same plane as the crystals of feldspar. It contains rare inclusions and is altered to chlorite.

The quartz crystal is interstitial or range of several crystals undulating extinction.

5. Analytical Techniques

5.1 Mineralogical Analyses

Major element compositions of minerals were determined in selected thin sections by EMA with a JEOL JXA 8900RL at the Universität-Göttingen. Acceleration voltage was set at 25Kv, beam current at 80 nA and beam diameter at 5µm. The detection limits, given as 2-sigma values of the background noise, range from 0.03 mass % (K_2O), 0.05 mass % (TiO_2, Al_2O_3, MnO, MgO, CaO, Na_2O) to 0.08 mass % (SiO_2) respectively. Natural minerals, synthetic oxides and pure metals are used as standards.

5.2 Whole-Rock Geochemical Analyses

Major elements analyses and trace elements of whole-rock samples were performed by inductively coupled plasma-mass spectrometry (ICP-MS) and X-ray fluorescence (XRF) at the Geowissenschaftlisches-Zentrun of Göttingen Georg-August-Universität, Abteilung Geochemie, Germany. Major elements and some trace elements (V, Cr, Ga, Rb, Sr, Zr, and Ba) were determined by XRF analysis on glass pills prepared with a lithium tetraborate flux. The analytical precision (2σ) is less than 1% for major elements (except for Fe, Na: 2%) and around 5% for trace elements. Additional trace elements (Li, Sc, Co, Ni, Cu, Zn, Nb, Sn, Hf, Ta, W, Pb, Th, U) and rare earth elements were analysed by ICP-MS. The analytical errors estimated according to rock standards JB3 and JA2 are about 15-20% for Nb and Ta, and < 10% for other trace elements.

5.3 Rb-Sr and Sm-Nd Isotopic Analyses

In the first step around 100 mg of the samples were digested by an acid mixture of HNO_3 and HF at a temperature of 180°C. The separation of Sr and REE was performed on columns filled with the cation exchange resin AG 50W-X8 with 2.5M HCl. Nd separation from the REE was performed on a column filled with Hexyl di-ethyl hydrogen phosphate (HDEHP) coated Teflon with 0.18M HCl. The isotopes of Sr and Nd were measured with a Finnigan TRITON mass spectrometer at the Geowissenschaftlisches-Zentrun of Göttingen

Georg-August-Universität, Abteilung Geochemie. Measurements were performed in static and in peak-jumping multicollector mode for Sr and for Nd respectively. Sr analyses were corrected for mass fractionation by normalization to $^{88}Sr/^{86}Sr = 8.375209$, while the Nd analyses were normalized to $^{146}Nd/^{144}Nd = 0.7219$. Repeated measurements of the standard NBS987 gave an average value of 0.710244, with a reproducibility of 0.000007 (2σ). The Nd standard La Jolla was determined with an average of 0.511845 ± 0.000005. The blanks were negligible, ranging, for Sr from 100 to 200 pg and for Nd around 100 pg.

6. Results

6.1 Mineralogy

Major element compositions of minerals were determined in selected thin sections, the results are represented in table 1.

Biotite is rich in iron [(23 ≤ FeOt ≤ 28%) and (0.73 ≤ Fe / Fe + Mg ≤ 0.77)], aluminium (14 ≤ 16% Al2O3), titanium ($TiO_2 \leq 2 \leq 4\%$) and has a mean concentration of magnesium (MgO ≤ 5 ≤ 8%, Table 1).

The biotites of Dschang granite have portray lepidomelane composition (Al= 2.7- 2.9), and plot near annite pole (Fig.4a). Their iron is highly comparable to those of biotite of the potassic subalkaline granitoids or monzonitic ferro-potassic association. This sub-alkaline character is also confirmed in the diagram Al_{tot} vs. Mg (Fig. 4b) Nachit et al. (1985). Compared to biotite granitoids of the Bafoussam region (Djouka-Fonkwé et al., 2008) and Ngondo Complex (Tagne-Kamga, 2003), they share the same peraluminous affinity as megacryst feldspar granite and, two mica granite of Bafoussam and the porphyritic granite of Ngondo complex.

Table 1. Selected microprobe analyses of biotite

	GD08					GD02											EDO2										
	1	2	3	4	5	6	7	8	9	10	11	12	13	14	15	16	17	18	19	20	21	22	23	24	25	26	27
SiO_2	35.68	35.34	35.41	35.72	35.81	34.77	35.44	35.20	35.59	35.17	35.47	35.34	35.33	34.95	35.50	35.54	36.00	36.01	35.73	35.63	36.21	35.69	35.38	35.59	36.03	35.49	35.57
Al_2O_3	14.95	14.71	14.93	14.81	15.56	14.74	15.06	15.12	15.13	15.53	15.11	15.09	14.93	14.61	14.96	14.45	15.02	14.82	15.00	14.55	14.93	14.92	14.41	15.07	15.26	14.61	15.04
TiO_2	3.42	3.19	4.28	4.30	3.01	4.06	3.62	4.24	3.53	3.75	4.15	3.65	3.97	3.83	3.81	4.10	4.39	4.51	3.72	4.41	3.91	4.15	4.37	3.43	3.89	4.23	3.88
Cr_2O_3	0.00	0.01	0.00	0.01	0.02	0.02	0.00	0.02	0.00	0.02	0.00	0.05	0.00	0.03	0.00	0.00	0.02	-0.04	0.00	0.01	0.00	0.00	-0.03	0.00	0.00	-0.02	0.00
Fe_2O_3	27.22	28.06	27.51	27.11	27.20	27.15	27.84	27.22	27.25	27.08	27.08	27.07	26.81	26.80	27.13	27.38	26.44	27.03	26.48	27.08	27.24	26.63	27.12	26.64	26.66	27.06	26.55
MnO	0.25	0.20	0.24	0.20	0.17	0.23	0.22	0.24	0.20	0.23	0.24	0.18	0.27	0.23	0.23	0.26	0.17	0.19	0.19	0.18	0.20	0.19	0.20	0.20	0.17	0.22	0.18
MgO	4.84	5.01	4.55	4.40	4.96	5.23	5.08	4.99	5.35	4.88	5.11	5.37	5.20	5.12	5.41	5.34	4.66	4.67	4.61	4.55	4.53	4.88	4.56	4.76	4.57	4.57	4.88
CaO	0.01	0.00	0.01	0.00	0.00	0.01	0.01	0.01	0.02	0.12	0.01	0.02	0.01	0.13	0.05	0.02	0.01	0.01	0.08	0.01	0.00	0.01	0.03	0.05	0.03	0.09	0.01
Na_2O	0.07	0.05	0.08	0.01	0.04	0.07	0.03	0.03	0.03	0.04	0.02	0.05	0.04	0.09	0.05	0.08	0.04	0.09	0.08	0.05	0.05	0.07	0.13	0.12	0.09	0.21	0.06
K_2O	9.59	9.28	9.54	9.59	9.62	10.01	9.89	10.07	9.84	10.10	10.07	9.67	9.83	9.41	9.89	9.88	10.13	10.13	9.92	10.06	10.24	10.14	9.90	10.07	10.16	10.02	10.15
BaO	0.09	0.06	0.08	0.14	0.13																						
NiO						0.00	0.00	0.03	0.02	0.00	0.00	0.02	0.00	0.01	0.02	0.00											
Total	96.10	95.90	96.60	96.30	96.50	96.28	97.20	97.16	96.95	96.91	97.26	96.52	96.40	95.22	97.06	97.04	96.86	97.47	95.81	96.53	97.33	96.67	96.09	95.93	96.86	96.52	96.30
Si	5.611	5.589	5.543	5.598	5.600	5.757	5.807	5.765	5.826	5.770	5.794	5.805	5.814	5.823	5.808	5.827	5.623	5.611	5.646	5.612	5.652	5.600	5.605	5.629	5.634	5.600	5.602
Al	3.035	3.003	3.020	3.000	3.139	2.877	2.910	2.919	2.920	3.004	2.909	2.922	2.897	2.869	2.887	2.794	2.764	2.720	2.793	2.700	2.747	2.758	2.690	2.808	2.812	2.716	2.791
Ti	0.449	0.422	0.560	0.563	0.393	0.506	0.446	0.522	0.435	0.463	0.510	0.450	0.491	0.480	0.469	0.505	0.515	0.528	0.442	0.522	0.458	0.489	0.520	0.408	0.457	0.502	0.459
Cr	0.000	0.001	0.000	0.001	0.003	0.003	0.000	0.002	0.000	0.002	0.000	0.006	0.000	0.004	0.000	0.000	0.002	-0.005	0.000	0.002	0.000	0.000	-0.003	0.000	0.000	-0.003	0.000
Fe	3.578	3.710	3.600	3.552	3.556	3.759	3.816	3.728	3.730	3.715	3.698	3.719	3.690	3.735	3.713	3.754	3.452	3.521	3.499	3.565	3.554	3.493	3.592	3.523	3.484	3.569	3.495
Mn	0.033	0.026	0.032	0.027	0.023	0.032	0.031	0.033	0.027	0.032	0.033	0.026	0.038	0.032	0.031	0.036	0.022	0.025	0.025	0.025	0.026	0.025	0.027	0.026	0.022	0.029	0.024
Mg	1.134	1.180	1.061	1.027	1.156	1.290	1.242	1.218	1.305	1.192	1.243	1.315	1.276	1.272	1.320	1.304	1.084	1.083	1.086	1.069	1.052	1.141	1.077	1.122	1.064	1.075	1.144
Ca	0.002	0.000	0.002	0.000	0.000	0.001	0.002	0.001	0.003	0.021	0.002	0.004	0.002	0.022	0.008	0.004	0.001	0.001	0.014	0.001	0.000	0.001	0.005	0.009	0.004	0.015	0.001
Na	0.021	0.017	0.024	0.004	0.012	0.022	0.010	0.010	0.010	0.012	0.006	0.016	0.013	0.030	0.017	0.025	0.013	0.026	0.023	0.015	0.015	0.020	0.038	0.037	0.027	0.063	0.017
K	1.923	1.872	1.905	1.917	1.919	2.113	2.067	2.104	2.054	2.114	2.098	2.027	2.063	2.000	2.065	2.067	2.018	2.012	2.000	2.021	2.038	2.029	2.000	2.031	2.026	2.016	2.039
Ba	0.006	0.004	0.005	0.009	0.008																						
						0.000	0.000	0.003	0.002	0.000	0.000	0.003	0.000	0.002	0.002	0.000											
Total	15.527	15.527	15.485	15.431	15.537	16.360	16.331	16.306	16.311	16.324	16.295	16.293	16.284	16.270	16.321	16.316	15.494	15.523	15.527	15.533	15.543	15.556	15.551	15.593	15.530	15.581	15.572
Fe/Fe+Mg	0.76	0.76	0.77	0.78	0.75	0.74	0.75	0.75	0.74	0.76	0.75	0.74	0.74	0.75	0.74	0.74	0.76	0.76	0.76	0.77	0.77	0.75	0.77	0.76	0.77	0.77	0.75

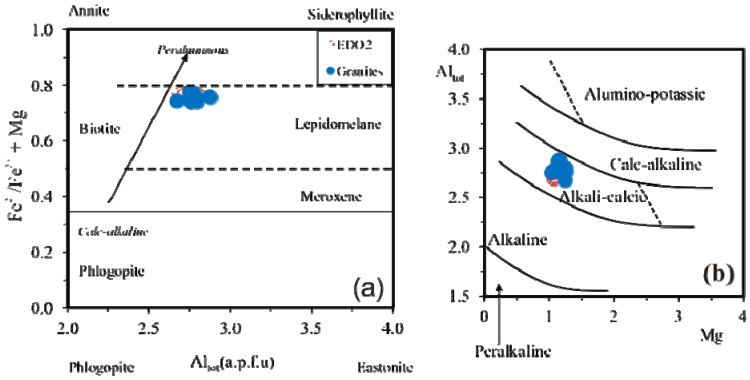

Figure 4. Biotite chemistry

(a) Biotite in the $Fe^{2+}/ (Fe^{+2} + Mg)$ vs Al_{tot}(a.p.f.u) coordinates of the annite-phlogopit-siderophyllite-eastonite quadrilateral. Subdivision after Deer et al. (1962) and Tröger (1982). Discrimination trends of biotite from calc-alkaline to peraluminous granitoid host rocks follows Abdel-Rahman (1994). (b) Al^{tot} vs Mg diagram of biotites after Nachit et al. (1985) showing alkali-calcic character of biotite of Dschang granite (Full circles, biotite granite; Open circle, Enclaves).

The value of Ti (a.p.f.u) for biotites enclaves varies from 0.41 to 0.53 and that of granites from 0.36 to 0.51 and X_{Mg} (Mg / Mg + Fe), 0.23 - 0.25 and 0.22 - 0.26 respectively, allow to assess the temperature of crystallization of biotite by the method of Henry (2005). On biotite enclave's temperatures vary from 680 ° C to 725 ° C while it ranges from 650 ° C to 750 ° C for the biotite granite. This interval of temperature corresponds to the one estimated in normative diagram Or-Ab-Qz of (Fig. 5f).

6.2 Classification

The samples analysed of the Dschang biotite granite lie on the boundary quartz monzonite and granite, but plenty in granite field (Fig. 5e). They are felsic rocks and display subalkaline, high-K calc-alkaline to shoshonitic affinity (Fig. 5a). They are also iron-bearing (Fe + Mg + Ti< 0.3; Fig. 5b) and weakly peraluminous I-type granitoids (A/CNK = 1 - 1.04; Fig. 6c). The biotite granites of Dschang are strongly fractionated granites (Fig. 5d). This degree of high fractionation justifies their shoshonitic affinity. These features of biotite granite of Dschang are comparable to haplogranites of Chappell (1999). All samples analysed are plotted around the minimum temperature melt composition, with the normative minerals Q, Ab and Or in Fig. 5f, that characterized felsic granites (haplogranites).

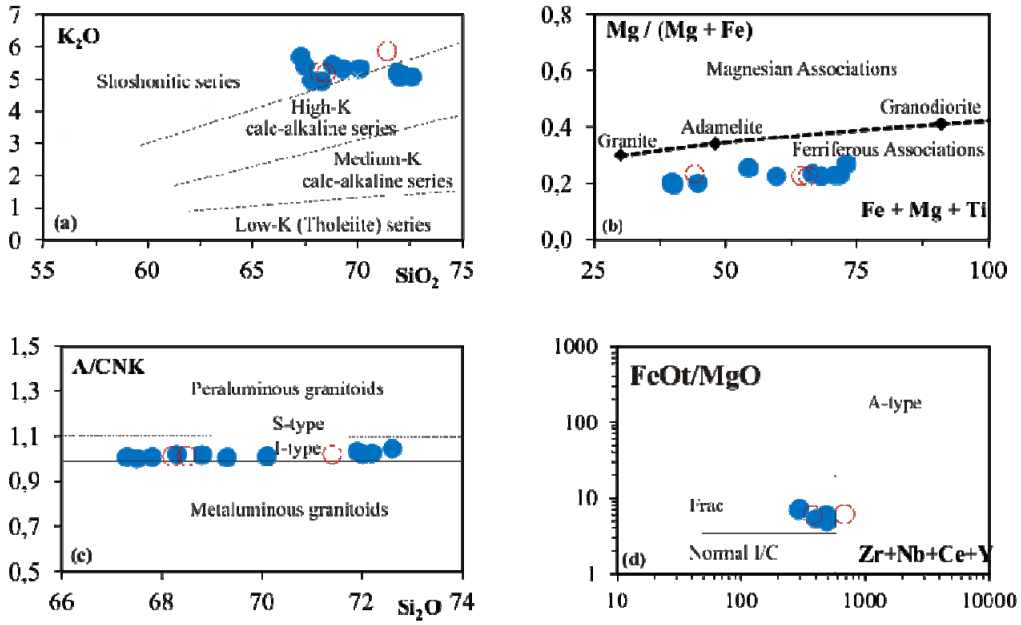

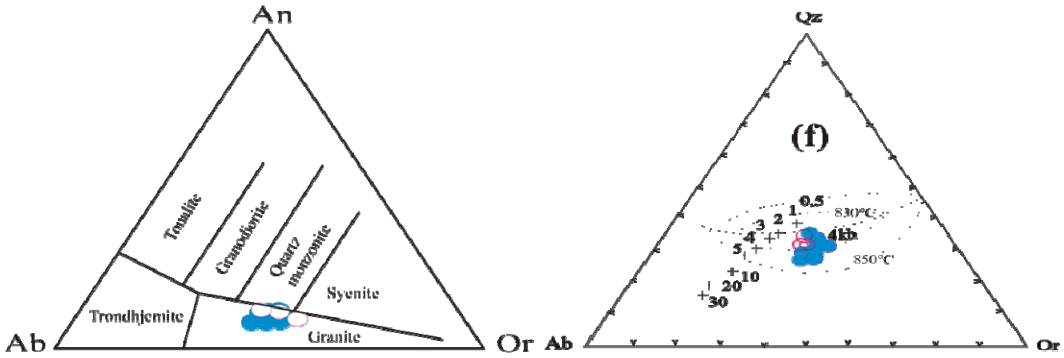

Figure 5. Biotite granite of Dschang in different diagrams of granitoid characterisation

(a) SiO_2 vs K_2O subdivisions are from Rickwood (1989); (b) discrimination between magnesian and ferriferous granitoids after Debon et Le Fort (1988); (c) SiO_2 vs $Al_2O_3/(CaO + Na_2O + K_2O)$ molar ratio, (Full circles, biotite granite; Open circle, Enclaves), boundary lines per-aluminous-metaluminous from Chappell and White (1992) and I-type – S-type granitoids from White and Chappell (1977); (d) Zr + Nb + Ce + Y vs FeOt/MgO discrimination diagram (Whalen et al., 1987), "Frac. Fractionated, Normal I/S, normal I and S-type granitoids; (e) Ab-An-Or norm classification of granitoid after O`Connor (1965); (f) Ab-Qz-Or norm estimated pression and temperature of granite crystallisation from Steiner et al. (1975), Cross are pressure in Kbar, minimum-melt compositions.

Table 2. Major and trace elements analyses

	Biotite Granite											Fine grain enclave		
Ech	G10	G11	GD08	GD09	GD10	GD07	GD04	GD01	GD02	GD05	GD06	ED06	ED02	ED01
SiO_2 (% wt)	72.20	67.30	72.00	68.80	67.50	69.30	68.30	71.90	67.80	72.60	70.10	71.40	68.50	68.20
TiO_2	0.27	0.51	0.31	0.47	0.59	0.44	0.51	0.28	0.52	0.28	0.35	0.28	0.49	0.50
Al_2O_3	14.10	15.80	14.00	15.20	15.40	14.80	15.30	14.20	15.00	14.10	14.60	14.20	15.00	14.90
Fe_2O_3	2.08	3.62	2.34	3.34	3.45	3.02	3.44	2.09	3.56	2.12	2.68	2.24	3.23	3.31
MnO	0.03	0.04	0.02	0.04	0.04	0.03	0.04	0.02	0.03	0.02	0.03	0.03	0.02	0.03
MgO	0.30	0.60	0.33	0.57	0.71	0.49	0.56	0.29	0.59	0.29	0.51	0.38	0.53	0.54
CaO	1.48	2.05	1.36	1.76	1.98	1.74	1.82	1.46	2.00	1.30	1.64	1.33	1.79	1.75
Na_2O	3.37	3.54	3.50	3.54	3.63	3.53	3.87	3.33	3.59	3.43	3.47	3.13	3.63	3.60
K_2O	5.10	5.68	5.05	5.45	5.40	5.32	4.93	5.18	4.95	5.06	5.32	5.87	5.17	5.20
P_2O_5	0.10	0.19	0.12	0.19	0.20	0.18	0.21	0.11	0.21	0.11	0.16	0.10	0.14	0.15
Total	99.07	99.32	99.02	99.36	98.9	98.88	98.94	98.78	98.2	99.26	98.85	98.98	98.5	98.15
K_2O/Na_2O	1.51	1.60	1.44	1.54	1.49	1.51	1.27	1.56	1.38	1.48	1.53	1.88	1.42	1.44
K_2O+Na_2O	8.47	9.22	8.55	8.99	9.03	8.85	8.80	8.51	8.54	8.49	8.79	9.00	8.80	8.80
FeOt/MgO	6.93	6.03	7.09	5.86	4.86	6.16	6.14	7.21	6.03	7.31	5.25	5.89	6.09	6.13
Fe*	0.87	0.86	0.88	0.85	0.83	0.86	0.86	0.88	0.86	0.88	0.84	0.85	0.86	0.86
Zr (ppm)	188	464	213	336	352	273	344	183	353	210	277	231	371	377
Y	10	11	8	10	14	8	15	11	13	8	8	10	17	18
Ba	851	1979	895	1304	1414	1317	1309	889	1562	815	1353	1344	1416	1439
Sr	206	540	200	279	322	269	267	209	313	182	336	238	270	273
Rb	185	141	187	195	196	191	214	187	201	170	182	201	168	170
Cr	8	11	9	13	17	12	10	12	9	9	10	9	11	8
V	13	21	14	19	22	19	22	15	16	12	17	13	21	14
Li	24.47			28.43	30.10					22.44	22.52	15.68	25.12	54.02
Sc	2.11			2.70	1.73					2.26	1.96	2.03	2.46	8.77
Co	2.50			4.72	5.66					2.50	4.64	2.90	4.53	15.90
Ni	17.02			29.75	36.79					19.12	23.78	18.73	33.27	87.61
Cu	6.31			8.23	10.59					6.22	7.51	6.61	7.92	31.20
Zn	44.23			87.46	90.76					60.51	65.98	53.96	96.85	180.51
Nb	13.32			18.99	14.78					12.91	9.75	15.09	26.59	32.13
Sn	1.17			1.27	5.05					0.93	0.76	1.20	0.86	3.06
La	41.79			65.07	56.65					37.06	60.28	53.58	143.36	113.58
Ce	79.99			122.45	109.43					64.33	106.98	125.78	270.20	186.13
Pr	7.85			11.62	9.44					6.91	10.02	10.02	25.64	20.43
Nd	26.29			41.55	31.21					23.28	34.44	34.77	85.32	73.38
Sm	4.80			6.64	4.66					3.93	4.79	5.66	14.92	12.82
Eu	0.97			1.58	1.31					1.17	1.31	1.25	2.00	3.28
Gd	4.06			5.68	4.22					3.38	4.18	4.90	12.79	11.17
Tb	0.45			0.56	0.42					0.38	0.38	0.51	1.09	1.16
Dy	1.45			1.63	1.24					1.14	0.91	1.56	3.30	4.34
Ho	0.28			0.30	0.25					0.24	0.20	0.32	0.53	0.75
Er	0.60			0.64	0.55					0.55	0.45	0.75	1.17	1.78
Tm	0.14			0.15	0.13					0.14	0.13	0.17	0.20	0.30
Yb	0.46			0.57	0.47					0.47	0.44	0.74	0.94	1.46
Lu	0.12			0.15	0.13					0.14	0.13	0.18	0.18	0.27
Hf	4.94			7.27	4.08					5.36	6.40	5.96	9.49	4.74
Ta	0.64			0.39	0.52					0.50	0.25	0.54	0.87	0.48
W	0.18			0.19	0.23					0.15	0.20	0.18	0.10	0.34
Tl	0.87			0.87	0.85					0.78	0.80	0.90	0.80	1.06
Pb	30.27			24.35	23.72					23.71	26.22	30.03	27.54	15.02
Th	20.23			18.62	11.95					11.54	17.27	26.22	43.35	11.80
U	1.21			1.25	0.92					1.23	1.38	2.08	1.55	1.75
Rb/Sr	0.90	0.26	0.94	0.70	0.61	0.71	0.80	0.89	0.64	0.93	0.54	0.84	0.62	0.62
Eu/Eu*	0.67			0.79	0.9					0.98	0.9	0.73	0.44	0.84

6.3 Major and Trace Elements

The SiO_2 content of the analysed samples varies from 67.3 to 72.6% correspondingly in contents of Al_2O_3 (14.2 - 15.8%), Na_2O (3.13 to 3.87%) and high K_2O (4.93 to 5, 87%), FeOt (2.08 to 3.62%) and medium CaO (1.30 – 2.05%) and lower MgO (0.29 – 0.71%), P_2O_5 (0.09 - 0.21%), TiO_2 (0.27 – 0.59%) (Fig. 6). K_2O/Na_2O (1.42 - 1.88) and FeOt/MgO (4.86 - 7.31) ratios are high. These geochemical characteristics are consistent with the mineralogical composition of these samples (abundant feldspar, poorly biotite content and some accessory minerals: titanite, allanite).

LILE concentrations are typically high, Ba (815 - 1979 ppm), Sr (182 - 540 ppm), Rb (141 - 214 ppm) and Zr (183 to 464 ppm), consistent with the fractionation of feldspar, biotite and zircon. In contrast, Nb (9.75 - 32.13 ppm) and Y (8 to 18 ppm) concentrations are low. The transition elements such as Ni (17.02 - 36.79 ppm), Co (2.5 - 5.66 ppm), Cu (6.22 -7.92 ppm), (except for the enclave EDO1 (Ni = 97.61 ppm, Co = 15.90 ppm, Cu = 31.20 ppm), have low contents reflecting the low concentration of ferromagnesian minerals in the granite.

The REE patterns of Dschang biotite granite look almost identical (Fig. 7a) except for the enclave EDO2 with high ΣREE (1296 ppm) and low Eu / Eu * = 0.44. The LREE are moderated fractionated ($(La / Yb)_N$ = 48 - 92 and exceptionally high (102) in the enclave EDO2)) relative to HREE. The profile of the HREE is flat ($(Dy / Yb)_N$ = 1 (2 in the enclaves)) suggesting their non-fractionation and the absence of residual garnet in the source. The spectra of standard trace elements (Fig. 7b) values of primitive mantle from Sun and Mcdonough (1989) show negative anomalies of Nb, Ta, Sr and Ti and enrichment in mobile elements (Ba, Rb, Th) comparable to the spectrum of the continental crust.

6.4 Rb/Sr and Sm/Nd Data

Five isotopic analyses of Sr and Nd whole rock have been carried out and results are presented in Table 3. The five samples form an errochron of 580 ± 110 Ma (initial $^{87}Sr/^{86}Sr$ of 0.7084 ± 0.0033, MSWD = 0.92, Fig. 8). This age is affected by a large error. However, it is comparable to the ages of syn-D3 granitoids of the Central Pan-African belt sufficiently documented along CCSZ (Nguiessi Tchankam et al., 1997; Djouka-Fonkwé et al., 2008; Kwékam et al., 2010; Kwékam et al., 2013).

Table 3. Sr and Nd isotopic data, TDM calcuted after Michard et al. (1985)

	Sr	Rb	$^{87}Rb/^{86}Sr$	$^{87}Sr/^{86}Sr$	2σ	$(^{87}Sr/^{86}Sr)_i$	Nd	Sm	$^{147}Sm/^{144}Nd$	$^{143}Nd/^{144}Nd$	2σ	$(^{143}Nd/^{144}Nd)_i$	$\varepsilon_{Nd600Ma}$	TDM (Ma)
GD02	313	201	1.858190	0.724229	0.000009	0.708303	46.35	7.50	0.097896	0.511384	0.000004	0.510999	-16.91	2112
GD05	182	170	2.702813	0.730552	0.000010	0.707372	23.28	3.93	0.102133	0.511449	0.000005	0.511047	-15.96	2104
GD06	336	182	1.567367	0.720530	0.000010	0.707101	34.44	4.79	0.084145	0.511365	0.000004	0.511034	-16.22	1923
GD09	279	195	2.022409	0.725369	0.000010	0.708033	41.55	6.64	0.096684	0.511383	0.000004	0.511003	-16.84	2093
GD10	322	196	1.761322	0.723625	0.000010	0.708530	31.21	4.66	0.090333	0.511313	0.000005	0.510958	-17.72	2073

The initial $^{87}Sr/^{86}Sr$ calculated at 600 Ma do not vary enough (0.7071 - 0.7085). As the Sr, reports $^{144}Nd/^{143}Nd$ remain constant (0.510954 -0.511047) suggesting a single homogeneous source for the biotite granite of Dschang. All analysed rocks presents ε_{Nd} strong negative values (-18 to - 16) with T_{DM} also old (1.9 to 2.1 Ga). These results indicate the contribution of Paleoproterozoic crust in the formation of Dschang biotite granite magma.

7. Discussion

7.1 Fractional Crystallization

Different Harker diagrams (Fig. 6) show a negative correlation between SiO_2 and Al_2O_3, Fe_2O_3, MgO, CaO, Na_2O, TiO_2, P_2O_5, Zr, Sr, Ba. Only K_2O and Rb show a slight dispersion probably related to post-magmatic disturbance. The negative correlation between the different elements and SiO_2 suggests that the crystallization of accessory minerals, biotite and feldspar controls the differentiation of biotite granite of Dschang. The negative anomaly in Eu (Eu/Eu* = 0.44 - 0.98) and Sr (Fig.7) confirms the role of plagioclase in this differentiation. Fractionated I-type granite feature observed in figure 5d is an additional argument to this view. However, moderated Eu/Eu* values indicate that this role is no significant, fractional crystallization is not only process. The presence of micro-enclaves, migmatitic structure, and the position of samples in figure 9a, suggest mixing of magmas from several sources. In addition, the tectonic context related to shear zone (CCSZ environment in a transpressional regime) has likely favoured the magma generation and their mixing follow the mechanism depicted by Duchesne et al. (2013) in the Maures massif (SE France).

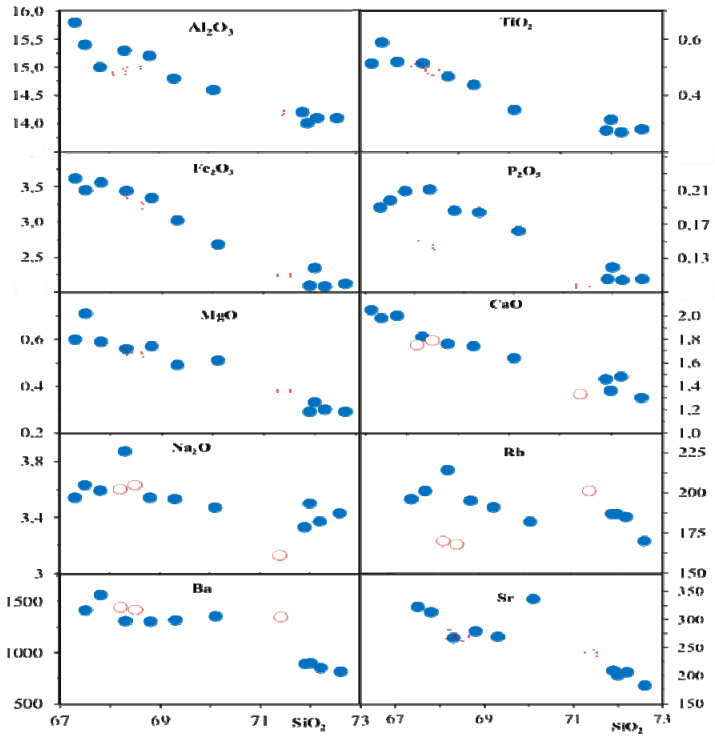

Figure 6. Harker diagram of some selected major and trace elements (Full circles, biotite granite; Open circle, Enclaves), major elements are in wt% and trace elements are in ppm as indicated in table 2

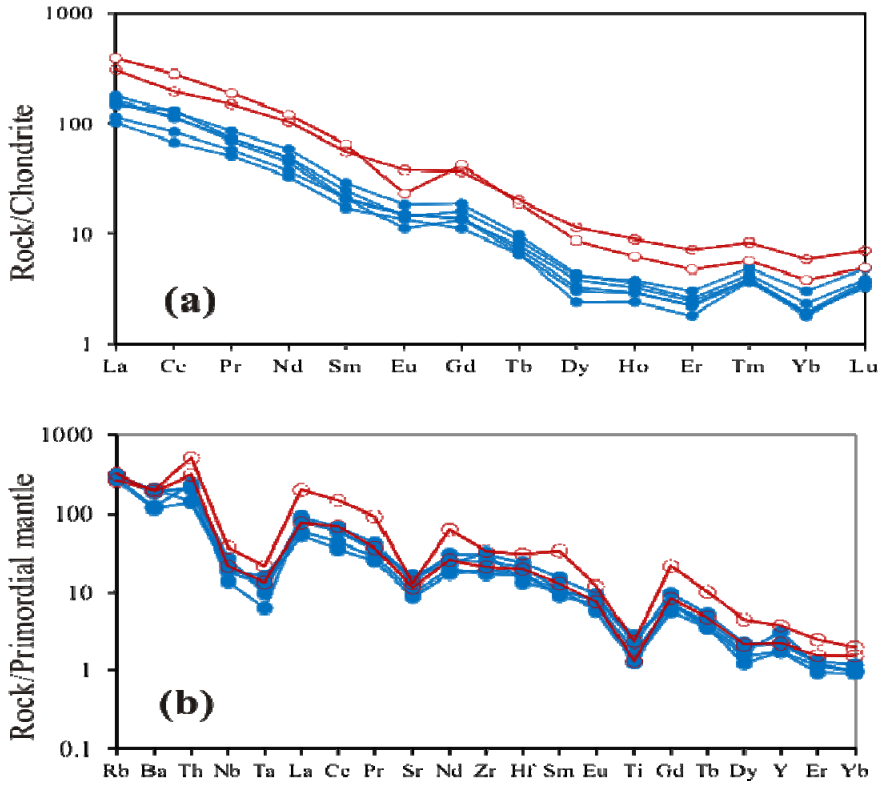

Figure 7.

(a) Rare Earth elements normalized to chondrites diagram after Nakamura (1974) and (b) spidergram normalized to primordial mantle (Sun et McDonough, 1989), (Full circles, biotite granite; Open circle, Enclaves)

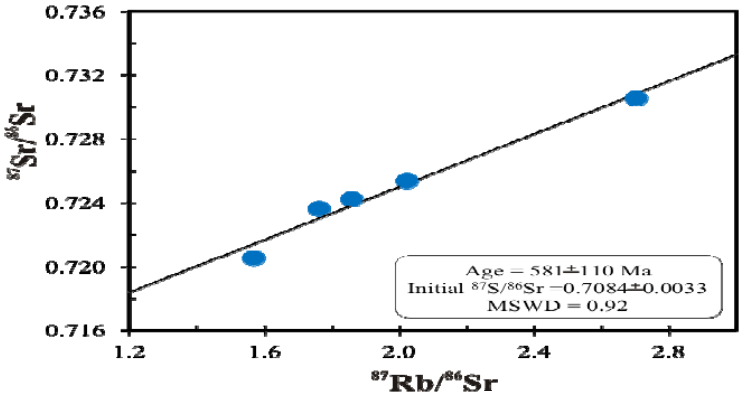

Figure 8. Isochron $^{87}Sr/^{86}Sr$ vs $^{87}Rb/^{86}Sr$diagram

7.2 Partial Melting and Source

The Rb/Sr ratios (0.26 - 0.90) are relatively high compared to that of the average crust (0.15) proposed by Rudnick and Gao (2004). The Ba/Rb ratios (5 to 8 with an average of 7) are close to that of the upper continental crust (7.47) and slightly higher compared to that of the average continental crust (9.3). The slight negative europium anomaly in the felsic rocks (SiO_2 = 67.3 - 72.6%, K_2O = 4.93 - 5.87%) and Sm/Nd (0.16 - 0.18, except GDO6 and GD10) fairly constant can be a result of high degree for partial melting (Terakado and Masuda, 1988). This partial melting reflected by the slight negative Eu anomaly in the granite and the strong negative europium anomaly of the enclave EDO2 (SiO2 = 68.5%, Sr = 273 ppm) can be regarded as the residue of partial melting. According to Chappell (1999), I-type haplogranites are formed under conditions where only the felsic components of the source rocks are fused, leaving the mafic components as a solid residue, which may have disengaged from the melt at or near the source, or later. The geochemical and mineralogical compositions of Dschang biotite granite are compatible with that of monzonitic subalkaline granitoids (Fig.4b and Fig.5a). K_2O/Na_2O values (1.27 to 1.88), $K_2O + Na_2O$ (8 to 9) and Fe* (0.83 – 0.88) combined with those of (Al_2O_3/CaO + Na_2O + K_2O molar) (Fig. 5c) indicate that the biotite granite of Dschang is the association of ferro-potassic subalkaline monzonite and peraluminous I-type granitoids (Fig. 5). Such I-type peraluminous granites generally derive from the consolidation of a granitic liquid formed by partial melting of former mafic meta-igneous rock, at the continental crust level (Roberts and Clemens, 1993; Barbarin 1999). The negative value of f (Sm / Nd) = (-0.57 to -0.48) <0 also suggests the importance of partial melting in the genesis of biotite granite of Dschang (Faure, 2001). These geochemical data corroborate the field observations (Orthogneiss xenolith and fine grained enclaves with residue habit, magmatization of the host gneiss). The Sr isotope data ($^{87}Sr/^{86}Sr_{600Ma}$ = 0706 to 0708) and Nd ($\varepsilon_{Nd600Ma}$ = -18 to -16) are additional arguments that the biotite granite of Dschang is formed from partial melting of old continental crust dates from Paleoproterozoic (T_{DM} = 1.9 to 2.1 Ga). The age of biotite and hornblende orthogneiss are about 739 Ma (Neoproterozoic), it is obvious that the biotite granite that have the same T_{DM} (1.5 to 2.1 Ga, Kwékam, 2005), can only come from the remobilization of Paleoproterozoic crust materials. The position of the analysed samples in the diagram $^{87}Sr/^{86}Sr$ vs ε_{Nd} (Fig. 9a), suggests a lower continental crust for the biotite granite protolith. Indeed, compared to Bafoussam and Ngondo granites, biotite granite of Dschang is in the field of crustal melts, on the extended the mantle line, while their counterparts (biotite granites or two micas granites) the Ngondo (Tagne-Kamga, 2003) and Bafoussam massive (Djouka-Fonkwé et al., 2008) plot on the mixing line between depleted mantle magmas and upper continental crust (McCullohand Chappell., 1982). In the latter case, Dschang biotite granite can be considered as the result from cooling mixing magmas.

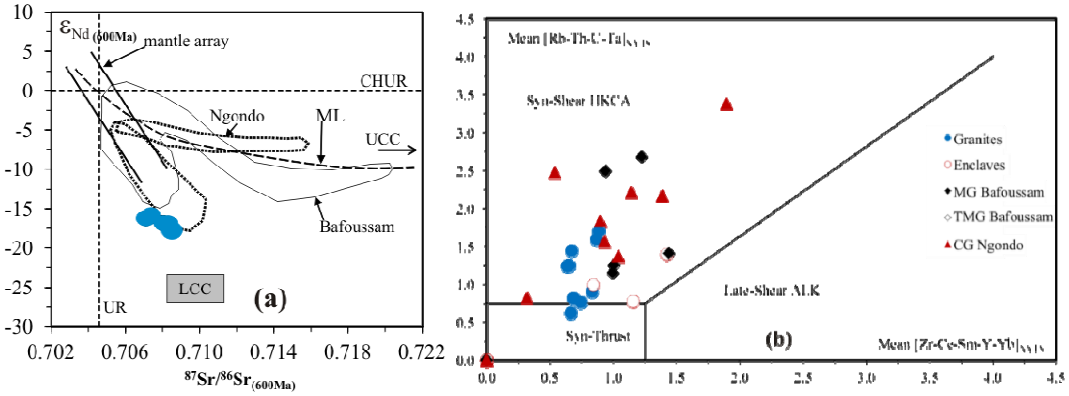

Figure 9.

(a) ε_{Nd}vs$^{87}Sr/^{86}Sr$ diagram, LCC, Lower continental crust and ; UCC, upper continental crust from Liégeois et al. (1998), Ngondo granites (Tagne-Kamga, 2003), Bafoussam granites (Djouka-Fonkwé et al., 2008), CHUR, chondritic uniform reservoir, UR, uniform reservoir, ML is mixing line between depleted mantle and continental crust sources recognized from Lachlan I- and S-type granitoids by McCulloch and Chappell (1982). (b) SNY (mean [Rb-U-Th-Ta] NYTS) vs SNX (mean [Zr-Ce-Sm-Y-Yb]NYTS) plot for the biotite granite of Dschang, Bafoussam (MG, megafeldspar and TMG, two micas) granite from Djouka-Fonkwé et al. (2008) and Ngondo coarse-grained granites (Tagne-Kamga, 2003); NYTS, normalization to the Yenchichi-Telabit series (Liégeois et al., 1998).

7.3 Geodynamic Context

The field structural observation materialised by N-S and NNE-SSW magmatic foliation stroked by ENE-WSW magmatic corridor, and all affected by ductile folding deformation in (NW-SE) anticlockwise motion testifies the syn-kinematic character of Dschang biotite granite. Plotting in the diagram [Zr-Ce-Sm-Y-Yb] NYTS vs. [Rb-Th-U-Ta] NYTS (Fig. 9b) of Liegeois et al. (1998), the biotite granite of Dschang and the granites of Bafoussam and Ngondo, all occupy the field of high-K calc-alkaline granitoids and shoshonitic (HKCA + SHO) which are syn-shear post-collisional granitoids. Indeed, the post-collisional period is known particularly as producing magmas from different sources (Liegeois et al. 1998), usually caused by very large movements along major deformation zones as transcurent faults (Example CCSZ). These movements can rapidly alter the structure and temperature of the lithosphere, both in the crust as the mantle (Liégeois et al., 1998). The recent works in West-Cameroon region consider the CCSZ as a transitional zone between Congo craton and a mobile zone (Liégeois et al., 2013; Kwékam et al., 2010; 2013; Tcheumenak Kouémo et al., 2014). This transitional zone is characterised by the delamination of the continental lithosphere (Liégeois et al. 2013). The model of lithospheric delamination was proposed to explain the genesis of high-K calc-alkaline and shoshonitic magmas (HKCA + SHO) in post-collisional setting (Liégeois et al., 2013; Kwékam et al., 2010; 2013). The NNE-SSW and ENE-WSW sinistral or dextral deformations in the biotite granite of Dschang are identical to those observed by Njiekak et al. (2008) in the Batié granite southeast of Dschang and Bafoussam northeast of Dschang; they are define as syn-CCSZ massive. The Ngondo massive (Tagne-Kamga et al., 1999) and Bandja (Nguiessi-Tchankam et al., 1997), as Fomopéa complex (Kwékam et al., 2010) have already been described as syn-CCSZ granitoids (Njanko et al., 2010). The mantle and/or crust origin of these clumps show that movements along the CCSZ have caused partial melting at various levels of the continental lithosphere of the region, melting of the mantle and/or continental crust, examples as plutons of Fomopéa (Kwékam et al., 2010); Ngondo (Tagne-Kamga, 2003); Bafoussam (Djouk-Fonkwé et al., 2008); Gabbro-Norite of Kekem (Kwékam et al., 2013). This process of production of the melts at different levels of the lithosphere, and their mixing during their ascent and emplacement are generally observed along several shear zone as indicated by Duchesne et al. (2013) on the Saint-Tropez peninsula granites.

8. Conclusion

The biotite granite of Dschang outcropping in the orthogneisses is weakly peraluminous haplogranite in composition from quartz monzonite to monzonite. Its biotite is peraluminous that crystallized under the temperature and pressure (650 -750°C at 4kbars) of common granites. Their sub-alkaline and shoshonitic affinity could result from its origin by partial melting of an older meta-igneous rock in continental crust. This partial

melting would be linked to the major movements along the central Cameroon shear zone which have contributed to the development of most syn-shear post-collisional granitoids in the central domain of the Central Africa Pan-African belt in Cameroon.

Acknowledgments

This study was performed during a stay of the first author in "Geowissenschaftliches Zentrun Göttingen, Universität-Göttingen", financed by the Germany Academic Exchange Organisation (DAAD). MK is grateful to Gerhard Wörner of “Universität-Göttingen" for his supervision. Anonymous reviewer have greatly improved the quality of the manuscript.

References

Abdel-Rahman, A. M. (1994). Nature of biotites from alkaline, calcalkaline and peraluminous magmas. *Journal of Petrology, 35*, 525–541. http://dx.doi.org/10.1093/petrology/35.2.525

Abdelsalam, M. G., Liégeois, J. P., & Stern, R. J. (2002). The Saharan metacraton. *Journal African Earth Sciences, 34*, 119-136. http://dx.doi.org/10.1016/S0899-5362(02)00013-1

Barbarin, B. (1999). A review of the relationships between granitoid types, their origins and their geodynamic environments. *Lithos, 46*, 605-626. http://dx.doi.org/10.1016/S0024-4937(98)00085-1

Castaing, C., Feybesse, J. L., Thieblemont, D., Triboulet, C., & Chevremont, P. (1994). Palaeogeographical reconstructions of the Pan-African/Brasiliano Orogen; closure of an oceanic domain or intracontinental convergence between major blocks? *Precambrian Research, 69*, 327–344. http://dx.doi.org/10.1016/0301-9268(94)90095-7

Chappell, B. W. (1999). Aluminium saturation in I- and S-type granites and the characterization of fractionated haplogranites. *Lithos 46*, 535-551. http://dx.doi.org/10.1016/S0024-4937(98)00086-3

Chappell, B. W., & White, A. J. R. (1992). I- and S-type granites in the Lachlan Fold Belt. Transactions of the Royal Society of Edinburgh: *Earth Sciences, 83*, 1–26. http://dx.doi.org/10.1017/S0263593300007720

Debon, F., & Le Fort, P., (1988). A cationic classification of common plutonic rocks and their magmatic associations: principles, method, applications. *Bull. Minéral, 111*, 493-510.

Deer, W. A., Homie, R. A., & Zussman, J. (1962). *An introduction to the rock-forming minerals* (2nd ed.). Springer, London, 696p.

Djouka-Fonkwé, M. L., Schulz, B., Schüssler, U., Tchouankoué, J. P., & Nzolang, C. (2008). Geochemistry of the Bafoussam Pan-African I- and S-type granitoids in western Cameroon. *Journal of African Earth Sciences, 50*, 148-167. http://dx.doi.org/10.1016/j.jafrearsci.2007.09.015

Duchesne, J. C., Liégeois, J. P., Bolle, O., Auwera, J. V., Bruguier, O., Matukov, D. I., & Sergeev, S. A. (2013). The fast evolution of crustal hot zone at the end of a transpressional regime: the Saint-Tropez peninsula granites and related dykes (Maures Massif, SE France), *Lithos, 162-163*, 195-220. http://dx.doi.org/10.1016/j.lithos.2012.12.019

Dumort, J. C. (1968). Carte géologique de reconnaissance à l'échelle du 1/50000, République Fédérale du Cameroun, Notice explicative sur la feuille Douala-Ouest, Direction des mines et de la géologie du Cameroun.

Faure, G. (2001). Origin of igneous rocks. Springer Verlag Berlin, Heidelberg, New York (Eds), 496p.

Frost, B. R., Barnes, C. G., Collins, W. J., Arculus, R. J., Ellis, D. J., & Frost, C. D. (2001). A geochemical classification for granitic rocks. *Journal of petrology, 42*(11), 2033-2048. http://dx.doi.org/10.1093/petrology/42.11.2033

Hadji, K. Z., Liégeois, J. P., Demaiffe, D., & Caby, R. (1998). The alkaline-peralkaline granitic post-collisional Tin Zebane dyke swarm (Pan-African Tuareg shield, Algeria): prevalent mantle signature and late agpaitic differentiation. *Lithos, 45*, 223-243. http://dx.doi.org/10.1016/S0024-4937(98)00033-4

Henry, D. J. (2005). The Ti-saturation surface for low-to-medium pressure metapelitic biotites: Implications for geothermometry and Ti-substitution mechanisms. *American Mineralogist, 90*, 316-328. http://dx.doi.org/10.2138/am.2005.1498

Kankeu, B., Greiling, R. O., & Nzenti, J. P. (2009). Pan-African strike-slip tectonics in eastern Cameroon-Magnetic fabrics (AMS) and structure in the Lom basin and its gneissic basement. *Precambrian Research, 174*, 258-272. http://dx.doi.org/10.1016/j.precamres.2009.08.001

Kankeu, B., Greiling, R. O., Nzenti, J. P., Bassahak, J., & Hell, V. J. (2012). Strain partitioning along the Neoproterozoic Central Africa Shear Zone system: magnetic fabrics (AMS) and structures from the Meiganga area, Cameroon. *Neues Jahrbuch für Geologie und Paläontologie Abhandlungen, 265*, 27-48. http://dx.doi.org/10.1127/0077-7749/2012/0244

Kwékam, M. (1993). Le massif plutonique calco-alcalin Pan-Africain de Fomopéa (Ouest Cameroun), Cadre structural - Pétrologie - Géochimie, Interprétation géodynamique. *Thèse Doctorat 3ème Cycle Yaoundé, I*, 155.

Kwékam, M. (2005). Genèse et évolution des granitoïdes calco-alcalins au cours de la tectonique panafricaine: le cas des massifs syn à tardi-tectonique de l'Ouest-Cameroun (régions de Dschang et de Kekem), *Thèse Doctorat d'Etat Université de Yaoundé, I*, 194.

Kwékam, M., Affaton, P., Bruguier, O., Liégeois, J. P., Hartmann, G., & Njonfang, E. (2013). The Pan-African Kekem gabbro-norite (West-Cameroon), U-Pb zircon age, geochemistry and Sr-Nd isotopes: Geodynamical implication for the evolution of the Central African fold belt. *Journal of African Earth Science, 84*, 70-88. http://dx.doi.org/10.1016/j.jafrearsci.2013.03.010

Kwékam, M., Liégeois, J. P., Njonfang, E., Affaton, P., Hartmann, G., & Tchoua, F. (2010). Nature, origin, and significance of the Fomopéa Pan-African high-K calc-alkaline plutonic complex in the Central African fold belt (Cameroon). *Journal of African Earth Science, 54*, 79-95. http://dx.doi.org/10.1016/j.jafrearsci.2009.07.012

Liégeois, J. P., Abdelsalam, M. G., Ennih, N., & Ouabadi, A. (2013). Metacraton: Nature, genesis and behavior. *Gondwana Research, 23*, 220-237. http://dx.doi.org/10.1016/j.gr.2012.02.016

Liégeois, J. P., Navez, J., Hertogen, J., & Black, R. (1998). Contrasting origin of post-collisional high-K calc-alkaline and shoshonotic versus alkaline and peralkaline granitoids. The use of sliding normalization, *Lithos, 45*, 1-28. http://dx.doi.org/10.1016/S0024-4937(98)00023-1

McCulloh, M. T., & Chappell, B. W. (1982). Ndisopic characteristics of S-type and I-type granites. *Earth and Planetary Sciences Letters, 58*, 51-64. http://dx.doi.org/10.1016/0012-821X(82)90102-9

Michard, A., Gurriet, P., Soudan, M., & Albarède, F. (1985). Nd Isotopes in French Phanerozoic shales: external vs internal aspects of crustal evolution. *Geochimica Cosmochimica Acta, 49*, 601–610. http://dx.doi.org/10.1016/0016-7037(85)90051-1

Nachit, H., Razafinahefa, N., Stussi, J. M., & Caron, J. P. (1985). Composition chimique des biotites et typologie magmatique des granitoïdes, *Comptes Rendus Académie Sciences Paris, 301*, 813-818.

Nakamura, N. (1974). Determination of REE, Ba, Fe, Mg, Na and K in carbonaceous and ordinary chondrites. Geochim. Cosmochim. *Acta, 38*, 757-775. http://dx.doi.org/10.1016/0016-7037(74)90149-5

Ngako, V. (1999). Les Déformations continentales panafricaines en Afrique Centrale. Résultat d'un poinçonnement de type himalayen. Doctorat d'Etat thesis, *University of Yaoundé, I*, Cameroon.

Ngako, V., Affaton, P., & Njonfang, E. (2008). Pan-African tectonic in northwestern Cameroon: Implication for history of Western Gondwana. *Gondwana Research, 14*, 509-522. http://dx.doi.org/10.1016/j.gr.2008.02.002

Nguiessi Tchankam Cl., Nzenti, J. P., Nsifa, E. N., Tempier, P., & Tchoua, F. (1997). A calc-alkaline magmatic complex from Bandja in the north-equatorial fold belt; a synkinematic emplacement of plutonic rocks in a sinistral strike-slip shear zone from pan-african age. *Comptes Rendus Académie Scieences Paris, 325*, 95-101.

Njanko, T., Nédélec, A., & Affaton, P. (2006). Synkinematic high-K calc-alkaline plutons associated with the Pan-African central Cameroon shear zone (W-Tibati area): petrology and geodynamic significance. *Journal of African Earth Sciences, 44*, 494-510. http://dx.doi.org/10.1016/j.jafrearsci.2005.11.016

Njanko, T., Nédélec, A., Kwékam, M., Siqueira, R., & Esteban, L. (2010). Emplacement and deformation of the Fomopéa pluton: Implication for the Pan-African history of Western Cameroon. *Journal of Structural Geology, 3*, 306-320. http://dx.doi.org/10.1016/j.jsg.2009.12.007

Njiekak, G., Dörr, W., Tchouankoué, J. P., & Zulauf, G. (2008). U-Pb zircon and microfabric data of (meta) granitoids of western Cameroon: Constraints on the timing of pluton emplacement and deformation in the Pan-African belt of central Africa. *Lithos, 102*, 460-477. http://dx.doi.org/10.1016/j.lithos.2007.07.020

O'Connor, J. T. (1965). Classification of quartz rich igneous rocks based on feldspar ratios. *US Geological Survey Professional Papers, 525B*, 79-84.

Penaye, J., Toteu, S. F., Tchameni, R., Van-Schmus, W. R., Tchakounté, J., Ganwa, A., Miyem, D., & Nsifa, E. N. (2004). The 2.1 Ga West Central African belt in Cameroon: extension and evolution, *Journal of African Earth Science, 39*, 159-164. http://dx.doi.org/10.1016/j.jafrearsci.2004.07.053

Penaye, J., Toteu, S. F., Van-Schumus, W. R., & Nzenti, J. P. (1993). U-Pb and Sm-Nd Preliminary geologic data on the Yaoundé séries Cameroon. Reinterpretation of the granulitic rocks as suture of a collision in the "Central African" belt. *Comptes Rendus Académie Sciences Paris, 317,* 789-794.

Rickwood, P. C. (1989). Boundary lines within petrologic diagrams which use oxides of major and minor elements. *Lithos, 22*, 247-263. http://dx.doi.org/10.1016/0024-4937(89)90028-5

Roberts, M. P., & Clemens, J. D. (1993). Origin of high-potassium, calc-alkaline, I-type granitoids. *Geology, 21*, 825-828. http://dx.doi.org/10.1130/0091-7613(1993)021<0825:OOHPTA>2.3.CO;2

Rudnick, R. L., & Gao, S. (2004). Composition of the continental crust. In: Rudnick R. L. (Ed.), *The crust, Treatise in Geochemistry, 3*, 1-64.

Steiner, J. C., Jahns, & Luth, R. H. (1975). Crystallisation of alkali feldspar and quartz in the halogranite system $NaAlSi_3O_8$-$KAlSiO_3O_8$-SiO_2-H_2O at 4 kb. *Bulletin Geological Society America, 86*, 83-98. http://dx.doi.org/10.1130/0016-7606(1975)86<83:COAFAQ>2.0.CO;2

Sun, S. S., & Mcdonough, W. F. (1989). Chemical and isotopic systematics of oceanic basalts: Implications for mantle composition and processes. In Magmatism in the Ocean Bassins (ed. A.D. Saunders and M.J. Norry), Geolo. Soc. Lond. *Special Publication,* 313-345

Tagne, K. G. (2003). Petrologenesis of the Neoproterozoic Ngondo plutonic complex (Cameroon, west central Africa): a case of late-collisional ferro-potassic magmatism. *Journal of African Earth Sciences, 36*(2003) 149-171. http://dx.doi.org/10.1016/S0899-5362(03)00043-5

Tagne, K. G., Mercier, E., Rossy, M., & Nsifa, N. E. (1999). Synkinematic emplacement of the Pan-African Ngondo igneous complex (west Cameroon, central Africa). *Journal of African Earth Sciences, 28*, 675-691. http://dx.doi.org/10.1016/S0899-5362(99)00038-X

Tchaptchet, T. D., Schulz, B., & Nzenti, J. P. (2009). Electron microprobe dating and thermobarometry of Neoproterozoic metamorphic events in the Kékem area, *Central African Fold Belt of Cameroon, Stuttgard, 186*, 95-109.

Tcheumenak, K. J., Njanko, T., Kwékam, M., Naba, S., Bella N. B. E., Yankeu, S. A. F., Fozing, E., & Njonfang, E. (2014). Kinematic evolution of the Fodjomekwet-Fotouni Shear Zone (West-Cameroon): implication on the emplacement of the Fomopéa and Bandja plutonic massifs: *Journal of African Earth Sciences, 99*, 261-275. http://dx.doi.org/10.1016/j.jafrearsci.2014.07.018

Térakado, Y., & Masuda A. (1988). Trace element variations in acidic rocks from the inner zone of southwest Japan. *Chem. Geol., 67*(1988) 227-241. http://dx.doi.org/10.1016/0009-2541(88)90130-1

Toteu, S. F., Penaye, J., & Poudjoum, D. Y. H. (2004). Geodynamic evolution of the Pan-African belt in Central Africa with special reference to Cameroon. Can. *J. Earth Sci., 41*, 73-85. http://dx.doi.org/10.1139/e03-079

Toteu, S. F., Van Schmus, W. R., Penaye, J., & Michard, A. (2001). New U-Pb and Sm-Nd data from north-central Cameroon and its bearing on the pre-Pan African history of central Africa. *Precambrian Research, 108*, 45-73. http://dx.doi.org/10.1016/S0301-9268(00)00149-2

Tröger, W. E. (1982). Optische Bestimmung der gesteinsbildenden Minerale, Teil 2. *Scheweizerbartsche Verlagsbuchhandlung, Stuttgart,* 822.

Whalen, J. B., Currie, K. L., & Chappell, B. W. (1987). A-type granites: geochemical characteristics, discrimination and petrogenesis. Contrib. *Mineral. Petrol, 95*, 407-419. http://dx.doi.org/10.1007/BF00402202

White, A. J. R., & Chappell, B.W. (1977). Ultrametamorphism and granitoids genesis. *Tectonophysics, 43*, 7-22. http://dx.doi.org/10.1016/0040-1951(77)90003-8